

OPTIMIZED SOLAR WATER PUMPING SYSTEM BASED ON AN INDUCTION MOTOR DRIVING A CENTRIFUGAL PUMP

A. Betka and A. Moussi

Abstract: This paper suggests how an optimal operation of a photovoltaic pumping system based on an induction motor driving a centrifugal pump can be realized. The optimization problem consists in maximizing the daily pumped water quantity via the optimization of the motor efficiency for every operation point, which has led to an optimum 'v-f' relationship useful in controlling the motor. This is reached via the control of a natural PWM VS inverter feeding the motor. The effectiveness of the proposed algorithm is described by simulation and the obtained results are compared to those of a system working with a constant air gap flux. The obtained results allow the improvement of the daily pumped water quantity and the pump efficiency. In addition, the influence of changing array temperature is also discussed.

Keywords : efficiency, photovoltaic, pumping, Optimization.

I. NOMENCLATURE

V	output generator voltage (v).
I	generator current (A).
I_{sc}	generator short-circuit current (A).
V_{th}	thermic voltage (v).
I_o	reverse saturation current (A)
R_s	series generator resistance (Ω).
I_{op}	optimum generator current (A).
V_{op}	optimum generator voltage (v).
V_{oc}	open circuit voltage (v).
P_M	maximum (optimum) generator power (w).
E	insolation (w/m^2).
t_{sr}	sunrise time (h).
t_{ss}	sunset time (h).
V_m	rms motor voltage (v).
r_1	stator resistance per phase (Ω).
r_2	equivalent rotor resistance per phase (Ω).
r_m	core loss resistance (Ω).
x_1	stator leakage reactance (Ω).
x_2	equivalent rotor leakage reactance (Ω).
x_m	magnetizing reactance (Ω).
x_{11}	stator cyclic reactance (Ω).
x_{22}	rotor cyclic reactance (Ω).
ω_s	angular frequency of the supply (rd/s).
ω_{sl}	slip speed (rd/s)
ω	motor speed (rd/s).
f	motor frequency (Hz).
p	pair pole number.
H	total head (m).
H_g	geodetic head (m).
Q	flow rate (m^3/h).
ρ	water volumic mass (kg/m^3).

II. INTRODUCTION

As the sources of conventional energy are dwindling fast with a corresponding rise in cost, considerable attention is being paid to other alternative sources. Solar energy which is free and abundant in most parts of the world has proven to be an economical source of energy in many industrial applications. The use of photovoltaic energy sources for water pumping and irrigation applications in remote areas of developing countries has also received considerable attention, since in many of these countries it is not economically viable to connect remote areas to the national electric grid. Such systems operate in open-loop speed control because precision and transient performance are not required. In addition, the system operates at steady state for long periods. A number of experimental pumping schemes, which are driven by DC motors [12-15], exist. It has been observed, however, that many of these schemes suffer from maintenance problems due to commutator and brushes presence. Since the use of brushless permanent magnet motors [18] is limited to low power PV systems due to their high cost, a pumping system based an induction motor fed either by a voltage source inverter [1-9] or current source inverter [5] has been proposed as an attractive alternative where reliability and maintenance can be guaranteed. Different optimization strategies have been proposed to improve the use efficiency of the generator such as maximum power tracking [16], motor efficiency optimization [4] and flow rate maximization [22-23].

The proposed scheme is a small scale system in which the photovoltaic array is directly coupled to an induction motor driving a monocellular centrifugal pump. This study fixes as a goal the maximization of the daily water pumped quantity obtained via the optimization of the motor efficiency since the flow-rate is monotonically increasing vs. the mechanical power at the shaft of a centrifugal pump [1]. This optimization is achieved by a proper adjustment of two liberty degrees: the motor frequency and modulation index of the PWM voltage source inverter feeding the motor. It is in fact a variable air-gap flux functioning. The obtained simulation results will be compared to those presented in [2] and [9] working with a constant air-gap flux. This study sets the value obtained by the amount of water flow per day as the criterion to evaluate the effectiveness of the algorithm, since in direct photovoltaic irrigation pump system we should preferably store the maximum quantity of the drawn water into a buffer tank before starting irrigation. In the derivation of the system equations, some assumptions are made. The motor is supposed to be unsaturated. The power losses in the inverter and stray losses in the motor are also supposed negligible. Furthermore, dynamic equations are not taken into

A.Betka is with the Electrical Engineering Institute, University of Oum El Bouaghi, Algeria, E-mail: a_betka@hotmail.com.

A.Moussi is with Lahryss laboratory, University of Biskra, Algeria, E-mail : moussi_am@hotmail.com

consideration since the system is assumed to run in steady state. In this paper, we will model each component of the system prior presenting the results via simulation. The main parts of the paper are organized as follows: Section 2 contains the description and modelling of the different components of the induction motor drive. In section 3, both the constant air-gap flux operation [2-9] and the proposed criterion of optimization are exposed, while in section 4, the results of simulation and interpretation are presented. In addition, the influence of changing cell temperature on the system performances is also investigated at the end of the section. This parameter can be regarded as a disturbance entree.

III DESCRIPTION AND MODELLING OF THE SYSTEM

The schematic diagram of the system analyzed in this paper is shown in Fig 1. It consists of a photovoltaic array, a natural sinusoidal PWM voltage source inverter and a three-phase squirrel cage induction motor driving a centrifugal pump. The specification of different components is illustrated in appendix.

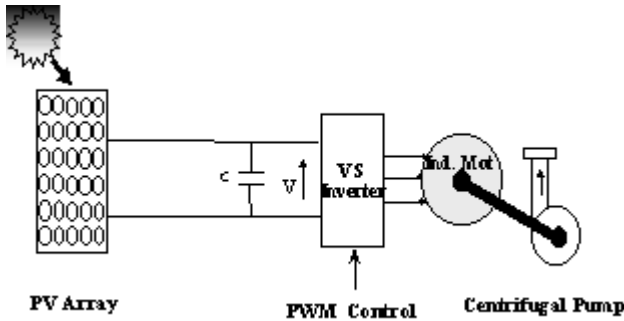


Fig.1 The PV Scheme Structure

III.1 Photovoltaic Generator Model :

Photovoltaic generators are neither constant voltage sources nor current sources but can be approximated as current generators with dependant voltage sources. The array considered in this study is a 16 series connected modules type AEG.40 where the I-V characteristic can be expressed as an implicit equation:

$$I = I_{sc} - I_0 \cdot \left(\exp\left(\frac{V + R_s \cdot I}{V_{th}}\right) - 1 \right) \quad (1)$$

The I-V curve is essentially influenced by the variation of two inputs: the solar insolation and the array temperature. The adaptation of equation (1) for different levels of solar insolation and temperature can be handled by the following equations:[7]

$$\Delta T = T - T_r \quad (2)$$

$$\Delta I = \alpha \left(\frac{E}{E_r} \right) \Delta T + \left(\frac{E}{E_r} - 1 \right) I_{sc} \quad (3)$$

$$\Delta V = -\beta \Delta T - R_s \Delta I \quad (4)$$

$$V = V_r + \Delta V \quad (5)$$

$$I = I_r + \Delta I \quad (6)$$

Where the suffix r refers to rated conditions given by $E_r = 1000 \text{ W/m}^2$ and $T_r = 25^\circ\text{C}$.

III.2 Inverter Model :

A natural PWM switching technique is used to drive the full bridge DC-AC inverter with a modulation index M and the ratio between the frequencies of the carrier and modulating waveforms P . In the present study, the carrier frequency is fixed at 750 Hz and P is set at $P = 15$ for the nominal insolation level $E = 1000 \text{ w/m}^2$. Consequently, the motor will be unaffected by the high order harmonics provided by the inverter for all the insolation levels since these harmonics which appear as sidebands centred around the switching frequency multiples (k.P.f) are naturally filtered by the motor itself. It is shown from [21] that for $P > 9$:

- The rms value of the fundamental motor voltage V_m is given by:

$$V_m = \frac{M \cdot V}{\sqrt{2}} \quad (7)$$

III.3 Three phase Induction Motor Model :

The steady state performance of the induction motor is modelled using the conventional equivalent circuit shown in Fig. 2.

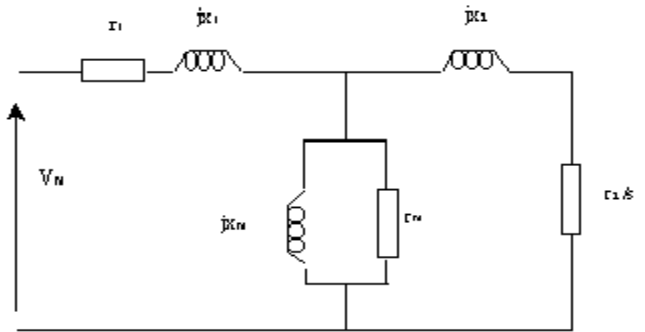


Fig. 2 Per Phase Equivalent Circuit

The input electric power is, then, given by :

$$P_{abs} = 3 \cdot R_{eq} \cdot \frac{V_m^2}{Z_{eq}^2} \quad (8)$$

Where Z_{eq} is the equivalent input impedance per phase :

$$Z_{eq} = R_{eq} + jX_{eq} \quad (9)$$

The mechanical equation is given by:

$$T_e = T_r + T_0 \cdot \omega \quad (10)$$

where the electromagnetic torque T_e is given by [21]:

$$T_e = 3 \cdot p \cdot \left(\frac{V_m}{\omega_s} \right)^2 \frac{\omega_{sl} \cdot \frac{X_m^2}{r_2}}{\left[r_1 - \frac{\omega_{sl}}{\omega_s \cdot r_2} (X_{11} \cdot X_{22} - X_m^2) \right]^2 + \left[X_{11} + \frac{\omega_{sl} \cdot r_1 \cdot X_{22}}{\omega_s \cdot r_2} \right]^2} \quad (11)$$

The centrifugal pump load torque T_r is assumed to be proportional to the square of the rotor speed:

$$T_r = C \left(1 - \frac{\omega_{sl}}{\omega_s} \right)^2 \cdot \omega_s^2 \quad (12)$$

C is a constant which depends on pump nominal data and T_o is the friction coefficient .

III.4 Centrifugal Pump Model :

The Flow-Head characteristic of a centrifugal pump can be approximated by quadratic form using Pfleider-Peterman model [23], in which the rotor speed ω is a parameter:

$$H = a_0 \cdot \omega^2 + a_1 \cdot \omega \cdot Q + a_2 \cdot Q^2 \quad (13)$$

where the motor speed ω is expressed as :

$$\omega = \left(1 - \frac{\omega_{sl}}{\omega_s}\right) \cdot \omega_s \quad (14)$$

a_0, a_1, a_2 are constants depending on the pump dimensions. The pump efficiency is defined as the ratio of the hydraulic power imparted by the pump to the fluid to the shaft mechanical power and is given by :

$$\eta_p = \frac{\rho g H Q}{C \left(1 - \frac{\omega_{sl}}{\omega_s}\right)^3 \omega_s^3} \quad (15)$$

The Q-H characteristic of the pipe network can be expressed by [22]:

$$H = H_g + \Psi Q^2 \quad (16)$$

Ψ is a constant which depends on conduit diameter and on all frictional losses of the pipe network.

III.5 Insolation Model :

A simplified approach was elaborated according to [8], and which will serve as a first approximative quantification of the incidental insolation. This model quantifies irradiance for a standard clear day:

$$E = E_M \sin(15(t - t_{sr})) \cdot \frac{\pi}{180} \quad (17)$$

The sunrise time is chosen as : $t_{sr} = 6 \text{ h.}00'$.

IV SIMULATION OF THE PV PUMPING SYSTEM

IV. 1 Constant Air-gap flux Operation [2-9] :

Generally, in variable speed drives, the motor air-gap flux is maintained constant at all frequencies so that the motor can deliver a constant torque. This will occur if the ratio V_m/f is kept constant at its nominal value. To compensate the voltage drop due to stator resistance effect at low frequencies, a boost voltage V_{mo} is added to the phase voltage. For aerodynamic loads, the stator voltage as function of frequency is given by :

$$V_m = V_{mo} + k \cdot f^n \quad \text{for } 0 \leq f \leq f_N \quad (18)$$

$$V_m = V_{mN} \quad \text{for } f \geq f_N \quad (19)$$

If $f > f_N$, the motor operates at constant power mode. For the concerned load, equation (18) that is depicted in **Fig. 3** is identified by the least square method for the constant :

$$V_{mo} = 6.3366 \text{ v} \quad k = 3.2485 \quad n = 1.0965$$

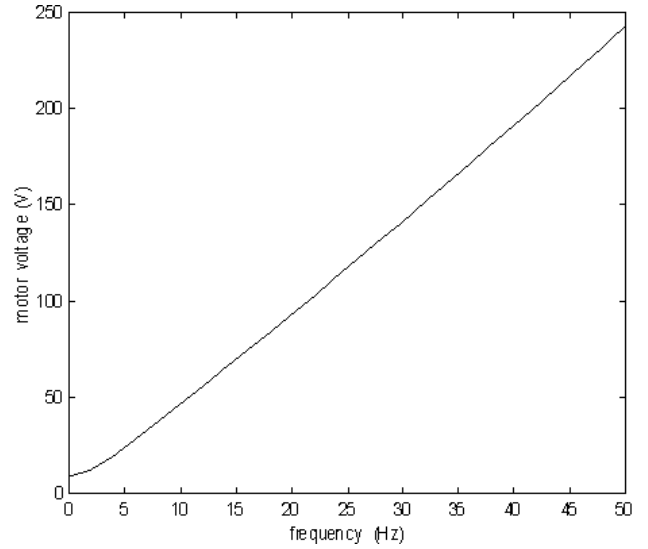


Fig. 3 Voltage - Frequency Relationship for Constant Air-gap flux Operation

To optimize the extracted electric energy, the PV array should always be operated close to its maximum output power. This will be obtained by setting up a linear relationship between the generator voltage and frequency :[9]

$$V = C_{10} + C_{11} \cdot f \quad (20)$$

If the system operates at array voltage values $V < V_{op}$ the motor speed ω presents a non-minimum phase response, and highly oscillating evolutions of ω are noticed [5]. To avoid such situation, the constant C_{10} should be greater than V_{op} for low frequencies. However, C_{11} which gives the curve slope should not be too small so as the operating point would not be far from the optimum one for high insolation values.

For the present study, constants are chosen as follow:

$C_{10} = 260 \text{ v}$ (corresponding to V_{op} of the insolation level $E = 100 \text{ w/m}^2$), and $C_{11} = 0.4$.

IV.2 Proposed Approach :

As demonstrated in induction motor theory, if the air-gap flux is kept constant for light loads (low torque values due to weak insolation levels in our case), an increase of iron losses is noticed, and consequently the motor efficiency falls as depicted in **fig. 4**. As a result, a significant degradation of the plant performances is remarked (flow rate, pump efficiency...etc).

In this paper, a correction of this efficiency by a variable air-gap flux operation is proposed and represented with the quotient V_m/f . This is reached by the optimization of a non-linear criterion representing the motor efficiency and by varying two degrees of freedom :

- The inverter frequency 'f'.
- The modulation index 'M'.

For an implementation, f indicates the frequency of the modulation waveform.

Optimization Criterion :

The maximization of the motor efficiency is chosen as the optimization criterion, which makes possible determining the momentary value of the vector :

$$X = [\omega_{sl} \ f \ I \ M]^T \quad (21)$$

optimizing the criterion:

$$J = \max f(X) \quad (22)$$

where $f(X)$ is the motor efficiency given by :

$$f(X) = \frac{C \cdot (1 - \frac{\omega_{sl}}{2\pi f})^3 \cdot (2\pi f)^3}{(V_{th} \cdot \ln(\frac{I_{sc} - I + I_0}{I_0}) - I \cdot R_s) \cdot I} \quad (23)$$

subject to the equality constraints :

$$g(X) = 0 \quad (24)$$

In addition, the generator current I and the modulation index M are limited as follows :

$$0 \leq I \leq I_{sc} \quad (25)$$

$$0 \leq M \leq 1 \quad (26)$$

The power balance of the system leads to the following expression:

$$\left(V_{th} \cdot \ln\left(\frac{I_{sc} - I + I_0}{I_0}\right) - I \cdot R_s \right) \cdot I = 3 \cdot \frac{R_{eq}}{Z_{eq}^2} \cdot V_m^2 \quad (27)$$

The equality constraints $g(X)$ are formed by the set of equation (1), (10), (20) and (27).

Optimization Method :

The nonlinear nature of the optimization criterion (23) as well as of the constraints calls for application of nonlinear programming methods.. At each iteration, the constrained problem (23), (24), is transformed to an other unconstrained one with linearised constraints using the Lagrangian function :

$$L(X, \lambda) = -f(X) + \sum_{i=1}^m \lambda_i \cdot G_i(X) \quad (28)$$

The solution is, then, carried out using the Quadratic Programming Algorithm, where G contains all the constraints, λ_i ($i=1, \dots, m$) are Lagrange Multipliers and m is the number of the constraints. The Hessian Matrix updating is made by the formula of Broyden, Fletcher, Goldfarb and Shanno (BFGS) [24].

After performing optimization, the daily pumped water quantity is defined as :

$$D = \int_{t_{sr}}^{t_{ss}} Q dt \quad (29)$$

The sunset time is chosen as : $t_{ss} = 18 \text{ h.00}'$.

V. SIMULATION RESULTS

The simulation is carried out on a system comprising a suction and a delivery tank, that are separated by a single pipeline. The volume of the two buffer tanks are respectively : 2.88 m^3 and 0.78 m^3 , while the geodetic head of the plant is: $H_g = 7.4 \text{ m}$. Figures 7 through 12 display system performances as function of insolation, which is considered as the simulation input, and for reference temperature $T_r = 25^\circ\text{C}$, using the proposed approach and that is described in [2-9].

In **Fig. 4**, the motor efficiency is displayed. It could be seen that an optimum efficiency $\eta_m = 73.6\%$ can be maintained using the proposed optimization technique. The control law given by equation (22) mainly governs the reduction of the frequency dependent losses (iron and friction losses). In fact, this represents an advantage as far as the system working with a constant air-gap flux [2-9] is concerned, especially for the insolation weak values ($E < 650 \text{ w/m}^2$).

Fig. 5 shows the pump flow-rate obtained by equalising equations (13) and (16). The pump succeed in overcoming the geodetic head H_g and throws water in the delivery tank only when a certain speed is reached ($\omega = 200 \text{ rd/s}$ in this case). The electric power threshold value corresponding to this limit is some watts less than 200 w ; about 20% of the rated motor power. This critical value is obtained at an insolation level $E_{th1} = 327 \text{ w/m}^2$ for the system working with the proposed optimization algorithm, whereas the system with constant flux do not contribute to water yield unless solar insolation exceeds $E_{th2} = 379 \text{ w/m}^2$. In addition, due to the proportionality existing between mechanical power on the shaft of a centrifugal pump and flowrate [23], the maximization of the motor efficiency, and hence of the mechanical power, leads to an increase of the flow-rate and consequently to a rise in the daily pumped quantity. By adopting the insolation model given by equation (17), and according to numerical integration of the equation (29), the obtained daily water amount is :

- $D = 28.84 \text{ m}^3$ for the constant air-gap flux technique [2-9].
- $D = 31.00 \text{ m}^3$ for the proposed approach.

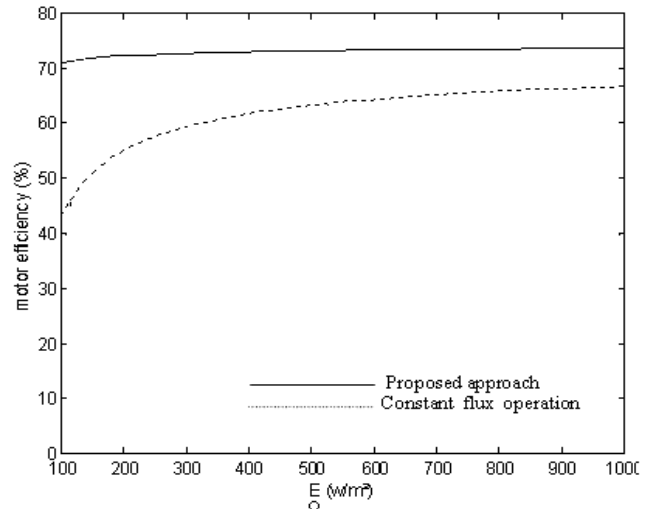


Fig. 4 Induction Motor Efficiency Curves

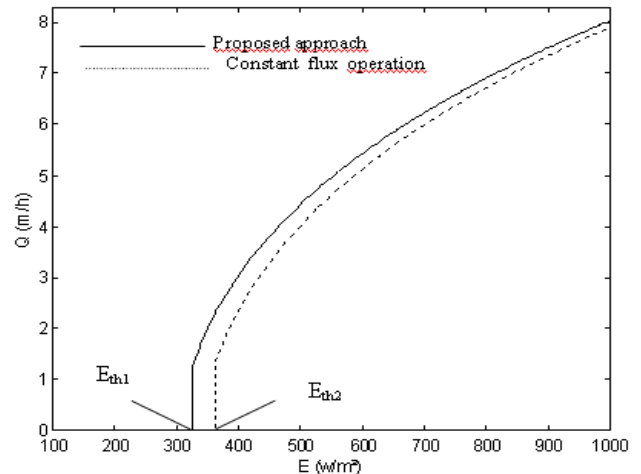


Fig. 5 Pump Flow-rate curves

Fig. 6 shows the improvement brought to the pump efficiency by the proposed technique. As can be seen, this improvement is more notable at insolation levels $E < 650$ w/m^2 . This increase inflicts the two following parameters:

- An increase of the total head H given by equation (13) as a result of the friction and shock losses reduction inside the pump.
- An increase of the flow-rate Q as a result of the leakage flow-rate decrease [9].

Consequently, the hydraulic power (p.g. $H.Q$) is increased.

Fig.7 illustrates the air-gap flux represented by the quotient (V_m/f) for the two studied systems. One can notice that the improvement of the motor efficiency is obtained by a field weakening, especially for low insolation values corresponding to low motor speed, and hence to weak load torques. This reduced flux yields essentially a motor iron losses decrease, since this kind of losses is flux-dependent. However, for the system [2-9], a nominal flux is permanently maintained ($V_m / f \sim 4.8$).

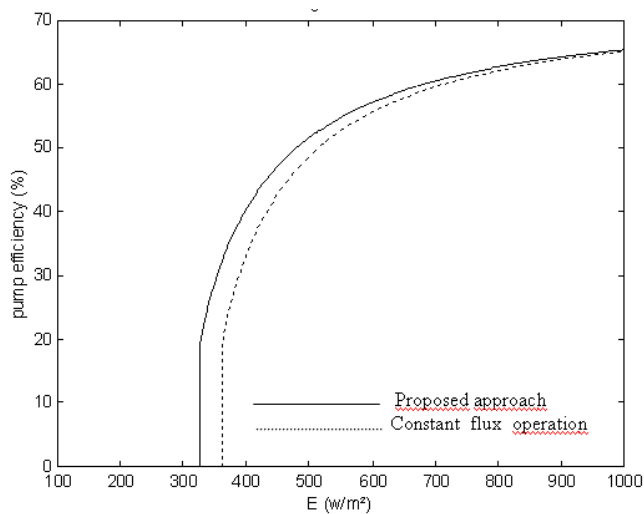


Fig. 6 Pump Flow-rate curves

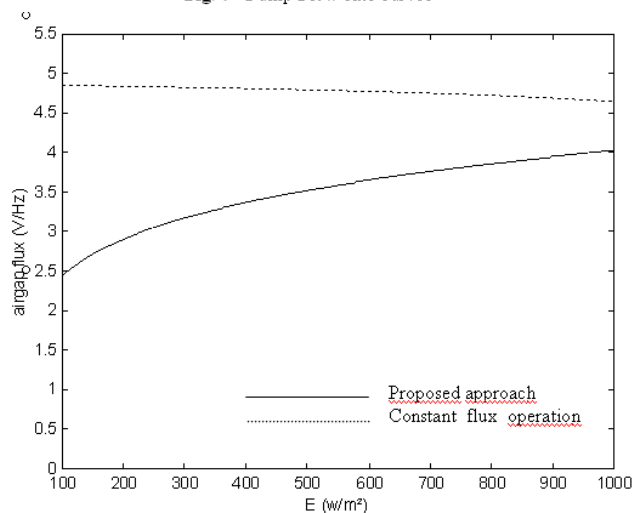


Fig. 7 Air-gap flux Characteristics

Fig. 7.b shows the voltage-frequency relationship, which can be viewed as the air-gap flux variation during the solar irradiance fluctuation the day long. As can be remarked, the voltage curve of the optimized system is always stated below that of the system with constant air-gap flux so to

keep the ratio (V_m/f) permanently less weighty, especially for the lowest insolation levels.

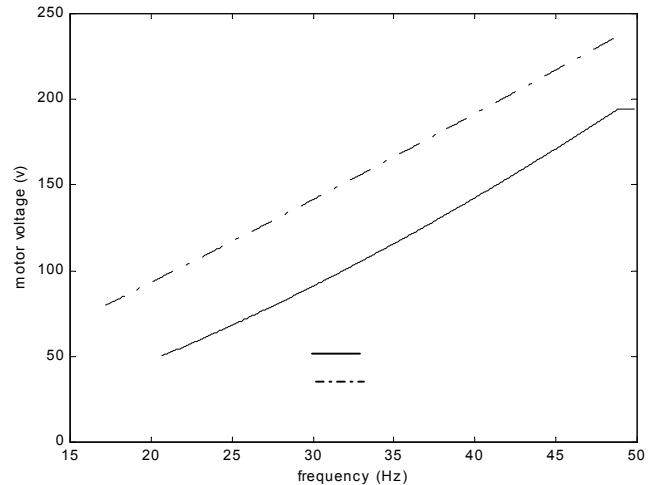


Fig.7b Voltage -frequency relationships

Fig.8 depicts the generator Power-Voltage characteristics and maximum power locus showed together with the consumed power in the case of constant air-gap flux mode, and field weakening mode that is proposed in our study. It is clear that for these two cases, the power consumed by the system is extremely close to the maximum one for high insolation values, and do not deviate significantly for lower values, bearing in mind that the Maximum Power Point Tracker is omitted. Consequently, the implementation will be less complex and less expensive.

In **Fig. 9a**, the modulation index M is presented, while **Fig. 9b** illustrates the output frequency f . One notices that the modulation index is reduced once the frequency falls, bringing therefore a decrease in the motor voltage V_m since the generator voltage is approximately constant (see figure 8). Consequently, the air-gap flux is reduced.

As a conclusion, the obtained results indicate that an enhancement of the system performance is obtained by the inclusion of the proposed optimization algorithm.

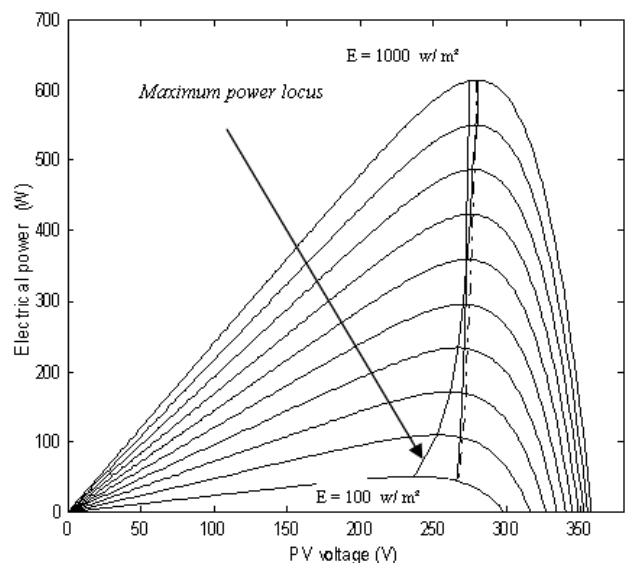


Fig. 8 Operating point locus for different insolation levels

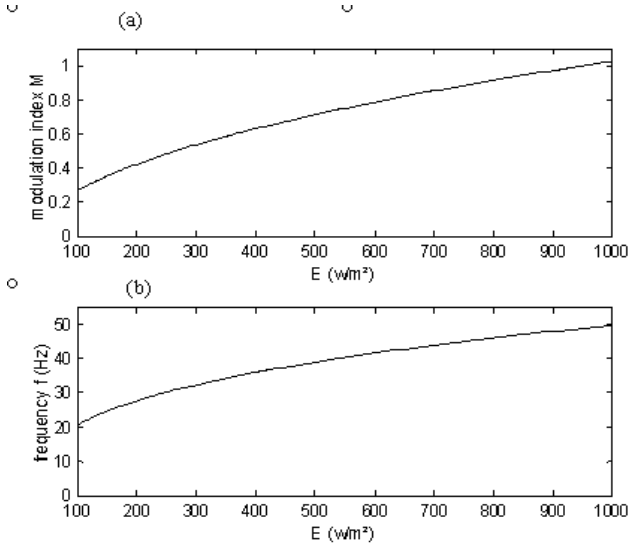


Fig.9 Modulation index and frequency curves

VI. Influence of Temperature Variation

As mentioned earlier in section 2, meteorological parameters, especially the array temperature, do not remain constant all day long, but change considerably. It is, then, worth investigating the influence of the daily average temperature variation on the predicted performances of the optimized system. In this case, the constant C_{10} showed by equation (20) is fitted as a function of temperature by the following expression :

$$C_{10} = 219.17 - 0.8743 \cdot T \quad (30)$$

Figures 10 through 13 display the simulation results as a function of insolation, obtained for three temperature values : $T = 0^\circ\text{C}$, $T = 15^\circ\text{C}$ and $T = 45^\circ\text{C}$. The geodetic head is set at : $H_g = 7.4$ m. As underlined in section 2, the decrease of temperature yields a significant increase of the electric power, and therefore of the motor speed. As a result, the mechanical power at the pump shaft, which varies with the cube of the motor speed, is improved. **Figure 10** illustrates the flow-rate curve. This latter implies that :

- As a consequence of the speed increase, the threshold electric power ($P_{eth} = 186$ w) required to start pumping is obtained at a lower insolation level E_{th} , as shown in **Table 1**, allowing the pump to convey water earlier in the morning and ceases later at the afternoon. Doing so, we improve the solar radiation utilisability defined as the ratio of the total insolation levels that exceed the threshold value to the total available insolation over the day [9]:

$$\mu = \frac{\int_{t_1}^{t_{ss}} (E - E_{th}) dt}{\int_{t_{sr}}^{t_{ss}} E dt} \quad (31)$$

t_1 is the hourly time when the insolation crosses the threshold level.

- The increase of the mechanical power as a consequence of the temperature decrease leads to an improvement of the flowrate and, then, to an elevation of the daily water amount, as shown in **Fig.11**.

Table 1 System Performance for variable Temperature

T (°C)	η_m (%)	η_p (%)	D (m³)	Flux (V/Hz)	E_{th} (w/m²)	μ (%)
0	43.65	65.69	32.38	4.03	308	91.34
15	73.63	65.29	31.00	3.81	320	90.67
45	73.59	64.28	27.96	3.36	349	88.71

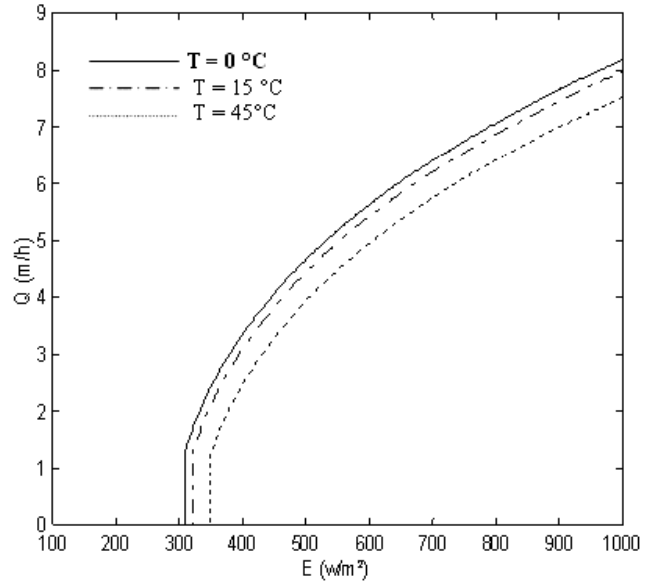


Fig. 10 Flow-rate Curves for variable Temperature

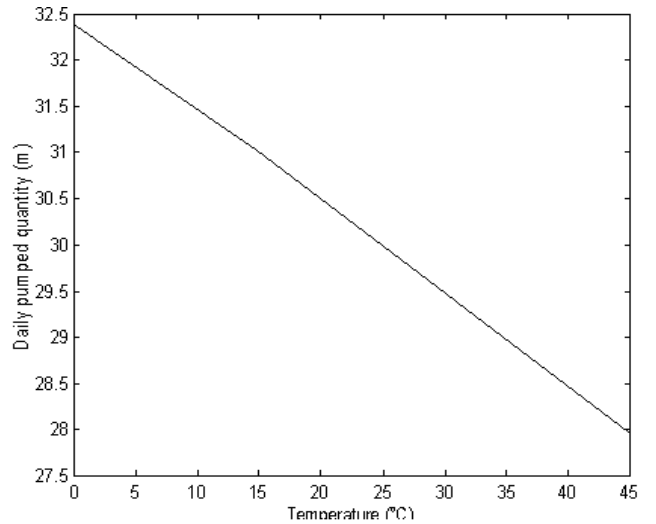


Figure 11 Daily Pumped Amount for variable Temperature

Fig.12 depicts the pump load torque, while in **Fig.13** the optimized air-gap flux is plotted. From these two curves, one can notice that for a given value of the incident insolation, the load torque decreases when the temperature goes up. The appropriate air-gap flux to optimize the motor efficiency tends to decrease, which confirm the following theoretical law : In case of an induction motor driving light loads, an optimum value of the motor efficiency is obtained with a weak air-gap flux [19].

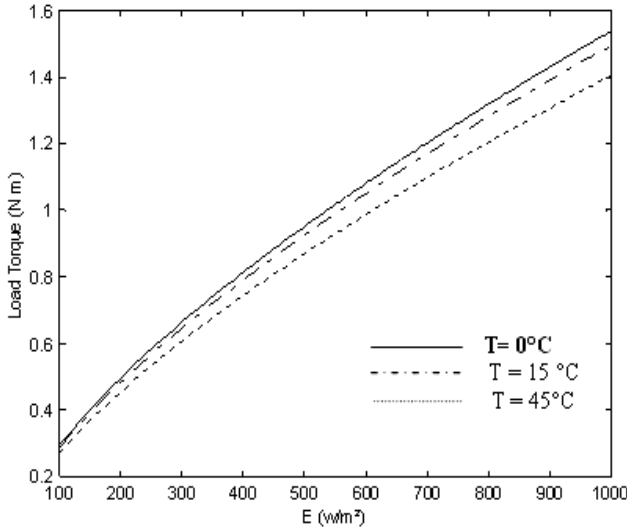


Fig. 12 Load Torque Curves

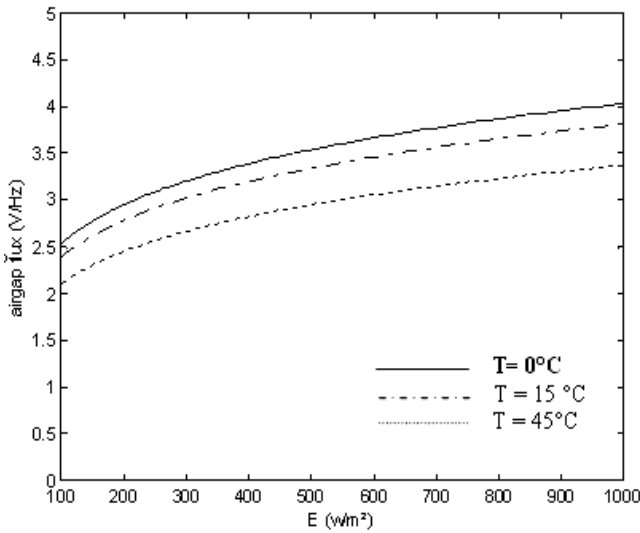


Fig. 13 Optimised Air-gap flux for variable Temperature

VII Economic Aspect:

To illustrate the economic performance brought by the proposed approach, the irrigated area by this solar pumping system is calculated under sahara climate conditions for two crops, namely potato and tomato. These are selected to meet with food standards of the site. The chosen application site to test the developed algorithm is Tamanrasset station. Tamanrasset lie at latitude 22.76° north and longitude 05.52° east. The altitude of the site is about 1377.0 m, and is located in one of the most dry regions of Algeria. April to November is normally the dry season and the wet season is from from December to May . The monthly average global irradiance collected for a Typical Meteorological Year varies between 5.17 kWh/m² /day and 7.61 kWh/m² /day as depicted in Fig.8. The average temperature of the site is 28°C.

Water needs and Calculation of the irrigated surface :

The vegetative cycle of the crop generally includes : initial phase, development, flowering and maturity phases. Water needs of the crops during each phase are commonly estimated using the evapotranspiration concept,

which results from soil evaporation and crop reference evapotranspiration (E_t) as follows [25]:

$$E_t = K_c \cdot E_{tr} \quad (32)$$

Where K_c is the crop coefficient.

E_t is obtained by the daily corrected –model of Penman[15], and the calculated values for the site of Tamanrasset is illustrated in fig. 14.

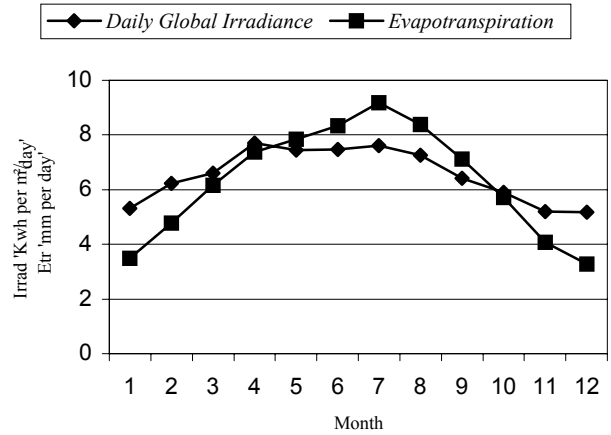


Fig.14 Daily global irradiance and reference evapotranspiration at the site of Tamanrasset

Table 2 and Table 3 shows respectively the sowing period and the crop coefficient for each vegetative phase for potato and tomato.

The total water needs over the vegetative cycle of the crop W_{tot} is the sum of the water needs of the four vegetative phases of the crop. The needed equation is :

$$W_{tot} = \sum_{k=1}^4 W_{ph}(k) \quad (33)$$

Where $W_{ph}(k)$ is the water needs for the vegetative phase k. The irrigated area S is the ratio between the volume of the pumped water during all the vegetative season D_{tot} and total water needs W_{tot} . The relationship is given by [25]:

$$S = \frac{D_{tot}}{W_{tot}} \quad (34)$$

Table2 Water needs and crop coeff versus vegetative phase of potato

Vegetative phase	N_{ph} (day)	K_c	W_{ph} (mm)
Phase 1	25	$K_{c11} = 0.40$	61.70
Phase 2	30	$K_{c21} = 0.52$ $K_{c22} = 0.89$	152.31
Phase 3	30	$K_{c31} = 1.15$	267.58
Phase4	20	$K_{c41} = 1.04$ $K_{c42} = 0.84$	148.11

Where N_{ph} is the number of days per phase, K_c is the crop coefficient per phase and K_{cij} is the crop coefficient for j sections of phase i.

Table3 Water needs and crop coeff versus vegetative phase of tomato

Vegetative phase	N_{ph} (day)	K_c	W_{ph} (mm)
Phase 1	30	$K_{c11} = 0.36$	79.70
Phase 2	40	$K_{c21} = 0.46$ $K_{c22} = 0.77$ $K_{c23} = 1.01$	232.58
Phase 3	45	$K_{c31} = 1.2$	474.30
Phase4	30	$K_{c41} = 1.01$ $K_{c42} = 0.74$	225.82

To illustrate the long performance of the proposed approach, the two presented algorithms were run for ten Typical Meteorological Years. The obtained pumped quantities and the irrigated field areas versus crop kind are depicted respectively in fig.15 and fig.16.

As can be seen, The calculated results of both the pumped quantities and consequently the irrigated fields of the proposed approach present a superiority where the system with constant air-gap flux is concerned. The benefit rate is 6.88% for potato and 6.78% for tomato. Therefore, the proposed optimization approach produces Prometheus performances, especially for low pumping heads.

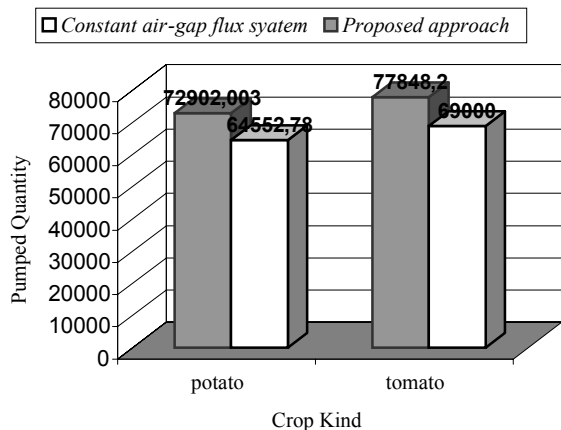


Fig. 15 Pumped volume (m³) for ten typical years versus crop kind

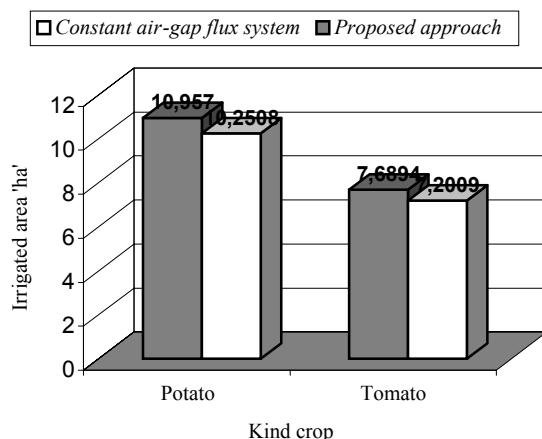


Fig. 16 Comparison between irrigated fields for ten typical years

Acknowledgement- The author wishes to thank Mr A.Hamidat, of the Algerian Renewable Energies Development Centre his valuable suggestions in Improving this work.

CONCLUSION:

This paper presents an optimal operation of a direct photovoltaic pumping system based on an induction motor. The optimisation criterion fixes the maximization of the motor efficiency, and where the extracted electric power is controlled by the inverter frequency instead of MPPT. A comparative study was led on the system described in [2-9]. The obtained simulation results show that an increase of both the daily pumped quantity and pump efficiency are reached by the proposed approach. In addition, the influence of the cell temperature variation on the performance of the optimized system was also investigated. It has been

concluded these performances are degraded once the temperature increases. As a result, the sizing of the system should be done in accordance with the average daily temperature of the site.

REFERENCES

- [1] S. R. Bhat, and al, ' Performance Optimization of Induction Motor-Pump System Using Photovoltaic Energy Source', IEEE Trans. on Ind App, Vol. 23, No. 6, 1987, pp: 995-1000.
- [2] M. N. Eskandar, A. M. Zaki, ' A Maximum Efficiency Photovoltaic-Induction Motor Pump System', Renewable Energy, Vol. 10, No. 1, 1997, pp: 53-60
- [3] R. Smith and al, ' Analysis and Performance of Novel Two-Phase Drive for Fan and Water-Pumping Applications', IEEE Trans on Ind App, Vol 36, No 4, November 1989.
- [4] B.N.Singh, and al, ' Optimized Performance of Solar Powered Variable Speed Induction Motor Drive', IEEE Trans. on Ind App, 1991.
- [5] O. Olorunfemi, 'Analysis Of Current Source Induction Motor Drive Fed From Photovoltaic Energy Source', IEEE Trans. on Energy Conv, Vol. 6, No. 1, 1991, pp: 99-106
- [6] Y. Yao, P. Bustamente and R.S. Ramshaw, ' Improvement of induction motor drive systems supplied by photovoltaic arrays with frequency control', IEEE Transactions on Energy Conv, Vol 9, No. 2, 1994.
- [7] D.Weiner and A.Levinson, 'water pumping optimal operation', Electrical machines and power systems, Vol 24, No. 3, pp 277-288, 1996.
- [8] K.Khousem and L.Khousem, ' optimum matching of direct-coupled electromechanical loads to a photovoltaic generator', IEEE Trans on Energy Conv, Vol 8, No.3, 1993.
- [9] R. Duzat, 'Analytic and Experimental investigation of a photovoltaic pumping system', PhD – work 2000, Oldenburg University Dissertation.
- [10] G. B. shrertha, L. Goel, 'A Study On Optimal Sizing Of Stand Alone Photovoltaic Stations' IEEE Trans on Energy Conv, Vol. 13, No. 4, 1998, pp: 373-377.
- [11] J. Samin and al. 'Optimal sizing of Photovoltaic Systems in Varied Climates', Solar Energy Vol. 6, o. 2, 1997, pp: 97-107.
- [12] M. M. Saied, 'Matching of DC Motor to Photovoltaic generator for Maximum Daily Gross Mechanical Energy', IEEE Trans on Energy Conv, Vol. 3, No. 3, 1988, pp: 465-471.
- [13] J. Appelbaum, ' Starting and Steady State Characteristics of DC Motor Powered by Solar Cell Generator', IEEE Trans on Energy Conv, Vol. 1, No. 1, 1986, pp: 17-25.
- [14] S. M. Alghuwainem, ' Steady State Operation Of DC Motors Supplied From Photovoltaic Generators With Step Up Converters', IEEE Trans. on Energy Conv, Vol. 7, No. 2, 1992, pp: 267-271.
- [15] M. Akbaba, and al, ' Matching Of Separately Excited Dc Motors To Photovoltaic Generators For Maximum Power Output', Solar Energy, Vol. 63, NO. 6, 1998, pp:375-385.
- [16] M. Veerachary, N. Yadaiah, ' ANN Based Peak Power Tracking For PV Supplied DC Motors', Solar Energy, Vol. 69, NO. 4, 2000, pp: 343-350.
- [17] R. Posorsky, ' Photovoltaic Water Pumps, An Attractive Tool For Rural Drinking Water Supply', Solar Energy, Vol 58 No 4-6, pp 155-163, 1996.
- [18] C. L. P. Swamy and al, ' Dynamic Performance of a permanent Magnet Brushless DC Motor Powered by a PV Array for Water Pumping', Solar Energy Materials and Solar Cells, Vol. 36, 1995, pp: 187-200

- [19] P. Famouri and J.J. Cathey, ' Loss Minimization Control Of An Induction Motor Drive', IEEE Trans. on Ind App, 1989, pp: 226-231.
- [20] W. Bucher, 'Improvements in Part Load Characteristics of Deep Well Pumps- Results of Comparative Field Tests', 12th European Photovoltaic Solar Energy Conference, Amsterdam, April 1994.
- [21] J.M.D. Murphy and F.G. Turnbull, ' power Electronics control of AC motors', Pergamon Press 1985.
- [22] A. Moussi, A.Betka and B. Azoui, ' Optimum design of a photovoltaic pumping system', UPEC99, Leicester UK, 1999.
- [23] A.Betka, A. Moussi, 'Optimisation of photovoltaic water pump coupled with an optimal PWM inverter', 47. Internationales Kolloquium, Ilmenau University, Germany, september, 2002.
- [24] R. Fletcher, 'A new Approach to variable metric algorithms', Computer Journal, Vol.13, 1970.
- [25] A. Hamidat, B. Benyoucef, T.Hartani 'Small-scale irrigated with photovoltaic water pumping system in Sahara regions', Renewable Energy, Vol. 28, 2003.

APPENDIX

Subsystem	Specification
Pump :	
Type	Centrifugal , Monocellular
Head	14 m
Flow rate	2.59 l/s
Speed	3000 rpm
Power	521 w
Pipe Network	$\Phi = 0.06 \text{ m}$ $H_g = 7.4 \text{ m}$
Motor :	
Type	three-phase induction motor
Voltage	380 v Δ
Current	2.5 A.
Power	1 Kw.
Speed	2880 rpm.
Resistances	$r_1=22.5 \Omega$ $r_2=7.87 \Omega$,
	$r_m=1.127 \text{ K } \Omega$.
Reactances	$x_1=x_2= 15.7 \Omega$, $x_m = 586 \Omega$
PV Array :	
Type	AEG-40 polycrystalline silicon
Peak power rating	614 w @ 280 v, 2.2 A.